Structure and Excitation Spectra of Third-Row Transition Metal Hexafluorides Based on Multi-Reference Exact Two-Component Theory

Ayaki Sunaga[1, 2]

[1] *ELTE, Eötvös Loránd University, Institute of Chemistry, Pázmány Péter sétány 1/A 1117 Budapest, Hungary*

[2] *Department of Physics, Graduate School of Science, Kyoto University, Kyoto 606-8502, Japan**

(Dated: June 9, 2024)

The structures and some vertical excitation energies of third-row transition metal hexafluorides (MF_6, M = Re, Os, Ir, Pt, Au, Hg) were calculated using the multi-reference configuration interaction (MRCI) theory based on exact two-component (X2C) Hamiltonian. The spin-orbit coupling (SOC) was variationally included at the Hartree-Fock level, enabling us to analyze the SOC at the orbital level. The excitation spectra were assigned based on the double group, a relativistic group theory applicable to states with the SOC. This study provides a fundamental understanding of the ligand field splitting, including the SOC, that is useful for the photochemistry and spin chemistry involving heavy elements.

I. INTRODUCTION

MX_6-type complexes, where M is a central metal element and X is a ligand, serve as excellent models for introducing ligand field splitting – an essential factor in predicting the electronic and spin states of transition metal complexes. This subject is frequently discussed in inorganic chemistry books [1–3]. While some MX_6 complexes exhibit the expected O_h symmetry based on their molecular formula, the Jahn-Teller (JT) effect [4, 5] can induce distortions that lead to another molecular structure such as D_{4h} symmetry. The smallest and most extensively reported MX_6 complexes would be MF_6. This complex garners attention not only in introductory chemistry texts but also due to its environmental impact of SF_6 [6, 7], notable oxidation properties when M is a third-row transition metal [8–10]) and UF_6 in nuclear fuel reprocessing [11, 12]. A comprehensive overview of the history and physical and chemical properties of MF_6 is provided in ref 13.

Traditional ligand field theory, developed for light elements, does not adequately capture the intricate electronic behaviors exhibited by heavy transition metals. The relativistic effect is significant when describing the chemistry of heavy elements [14–19]. The relativistic effect can be classified into the following two effects: i) scalar relativistic effect, where the s and p orbitals are contracted while the d and f orbitals are expanded, and ii) spin-orbit coupling (SOC), which is the interaction of the electron spin and the magnetic field induced by a charge in relative motion, leading to the splitting of the degenerate orbitals with $l \geq 1$, where l is the quantum number of the electronic angular momentum. The former effect can be sufficiently taken into account by introducing a pseudo-potential [20–23], where core electrons are replaced with a fitted potential for valence molecular properties. The latter effect can become small in molecules with low symmetry even if heavy elements are included because of the orbital angular momentum quenching [1, 3, 24], and thus this effect can often be ignored. However, the SOC can become significant and has to be carefully considered in complexes with high symmetry, which is the target of our study.

Another important aspect is including static correlation effects to treat the degeneracy in the MF_6 molecules. Most previous studies of MF_6 [25–38] were based on single-reference methods such as the density functional theory (DFT) or coupled cluster theory. These methods are sufficient for closed-shell systems but may encounter problems when there is significant multi-reference effect In the context of the vibrational coupling with the JT effect, multi-reference methods with the SOC were employed by Balasubramanian's group for metal clusters [39–42], by Mondal for the first-row transition-metal trihalides 43, 44, and by Koseki's group for third-row transition-metal tetrahydrides [45, 46]. However, such an approach has not been applied for MF_6 molecules.

The static JT distortion itself is well known in the structures of MF_6 molecules with non-zero spin. However, the structure of the third-row transition metal hexafluorides may be stable in the presence of JT distortion. It is currently recognized that ReF_6 and OsF_6 show the dynamic JT effect [47–49], and the structures of ReF_6, OsF_6, IrF_6, and PtF_6 are very close to O_h based on electron-diffraction experiments in the gas phase [50–52], single-crystal X-ray diffractometry [53], and extended X-ray absorption fine structure (EXAFS) [54]. Even if it exists, the JT distortion may be smaller than experimental errors. In theory, the most sophisticated calculation for the third-row transition metal hexafluorides was carried out at the coupled cluster singles and doubles with perturbed triples (CCSD(T)) level with the SOC at the DFT level [33]. Their calculated structures agree with the experiment well, but they compared the averaged bond lengths of the D_{4h} structures and experimental structures in O_h symmetry. It was reported that the SO effect stabilizes the O_h structures of PtF_6 [55, 56] and

* sunagaayaki@gmail.com, ayaki.sunaga@ttk.elte.hu

IrF_6^- [57] based on four-component DFT and CCSD(T) methods, respectively. However, a systematic study for third-row transition metal hexafluorides based on relativistic multi-reference theory has not been reported.

In this study, the effect of the SOC in third-row transition metal hexafluorides is extensively investigated. The multi-reference configuration-interaction (MRCI) method based on the exact two-component Hamiltonian is employed to calculate the structures and vertical excited energies. The calculated electronic excited states, including the SOC, are assigned based on the double group, which is a relativistic group symmetry, taking the SOC into account. The schematic diagrams based on the one-electron orbital Figure 1 are also proposed.

II. THEORY

Assigning the symmetry of MF_6 in the relativistic framework requires the double group, which is a relativistic symmetry group. Although the double group is well known [16, 24, 58–60], we briefly describe it to clarify the notation in this work.

An operator for a rotation by a finite angle ϕ about the quantization axis can be expressed as follows [61, 62]:

$$\hat{R}_z(\phi) = \exp\left(\frac{-i\hat{J}_z\phi}{\hbar}\right), \tag{1}$$
$$\hat{R}_z(\phi)|J, M_J\rangle = \exp\left(-iM_J\phi\right)|J, M_J\rangle,$$

where i is the imaginary unit, J is an angular momentum (whether orbital, spin, or total angular momentum) and M_J is the projection of the angular momentum along the axis z. The representation matrix of this rotation with respect to the basis $M_J = -J, -J+1, \ldots, J$ can be expressed by

$$\mathbf{D}^J\left(R_\phi\right) = \begin{pmatrix} \exp[iJ\phi] & 0 & \ldots & 0 \\ 0 & \exp[i(J-1)\phi] & \ldots & 0 \\ \ldots & \ldots & \ldots & \ldots \\ 0 & 0 & 0 & \exp[-iJ\phi] \end{pmatrix} \tag{2}$$

A trace of this matrix is

$$\chi^J\left(\phi\right) = e^{-iJ\phi}\sum_{l=0}^{2J}\left(e^{i\phi}\right)^l = \frac{\sin[(J+1/2)\phi]}{\sin(\phi/2)}. \tag{3}$$

This is the character of the representation $\mathbf{D}^J\left(R_\phi\right)$ with respect to the rotation ϕ. For example, in the case of $R_\phi = C_4$ ($\phi = \pi/2$) and $J = 1/2$, $\chi^J\left(\phi\right) = \sqrt{2}$ is obtained.

The periodicity of eq 3 can be obtained for the cases where J is an integer or a half-integer:

$$\chi^J\left(\phi \pm 2\pi\right) = +\chi^J\left(\phi\right);\ \text{(an integer } J\text{)}, \tag{4}$$
$$\chi^J\left(\phi \pm 2\pi\right) = -\chi^J\left(\phi\right);\ \text{(a half-integer } J\text{)}, \tag{5}$$
$$\chi^J\left(\phi \pm 4\pi\right) = +\chi^J\left(\phi\right);\ \text{(an integer/a half-integer } J\text{)}, \tag{6}$$

In the non-relativistic (NR) case, the molecular symmetry is described by the spatial symmetry and the electronic orbital angular momentum ($M_J = M_L$). In thfis case, the quantum number ($J = L$) is an integer, and rotation by 2π returns the system to the original state (eq 4). That is, rotation by 2π is equivalent to the identity operator $\hat{E}$. This is the case of a normal point group. Meanwhile, in the relativistic case, the projection of the total angular momentum $M_J = M_L + M_S$ is a good quantum number, and J becomes a half-integer when the system contains an odd number of electrons. Here, rotation by 2π reverses the sign (eq 5). In both cases, $\hat{R}_{\phi=4\pi} = \hat{E}$ is satisfied.

The symmetry operations in the double group are obtained from the direct product of the point group and the group $\left\{\hat{E}, \hat{Q}\right\}$, where $\hat{Q} = \hat{R}_{\phi=2\pi}$. Several columns are added to the character table to describe additional irreducible representations that correspond to the odd-number electron systems. $\hat{Q}$ does not disturb the point group (cf. eq 4) and only affects the additional irreducible representations (cf. eq 5).

The great orthogonality theorem also holds in the double group. Hence, the direct product of irreducible representations and the reduction of the reducible representation can be performed as the point group. For example, the splitting of the one-electron molecular orbitals belonging to the irreducible representations e_g and t_{2g} in O_h symmetry due to the SOC in the double group can be expressed as follows:

$$e_g \otimes e_{1/2,g} = u_{3/2,g}, \tag{7}$$
$$t_{2g} \otimes e_{1/2,g} = u_{3/2,g} \oplus e_{5/2,g}. \tag{8}$$

Here $e_{1/2,g}$ is the representation of the electron spin in the double group.

In the electronic structure theory, the SO splitting of the states is found when the total spin is nonzero. In the case of group theory, however, whether J is an integer or a half-integer is important (cf., eqs 4 and 5). Even when the SOC contributes, if J is an integer (that is, an even number of electrons in the system), the representation of the system is the same as the point group of the NR case. The double group is applied only when the number of electrons is odd.

III. COMPUTATIONAL DETAIL

All calculations of this study were carried out by using a development version of the DIRAC program [63, 64]; the precise version and build information are shown in the output files, see ref [65]. Our calculations are based on

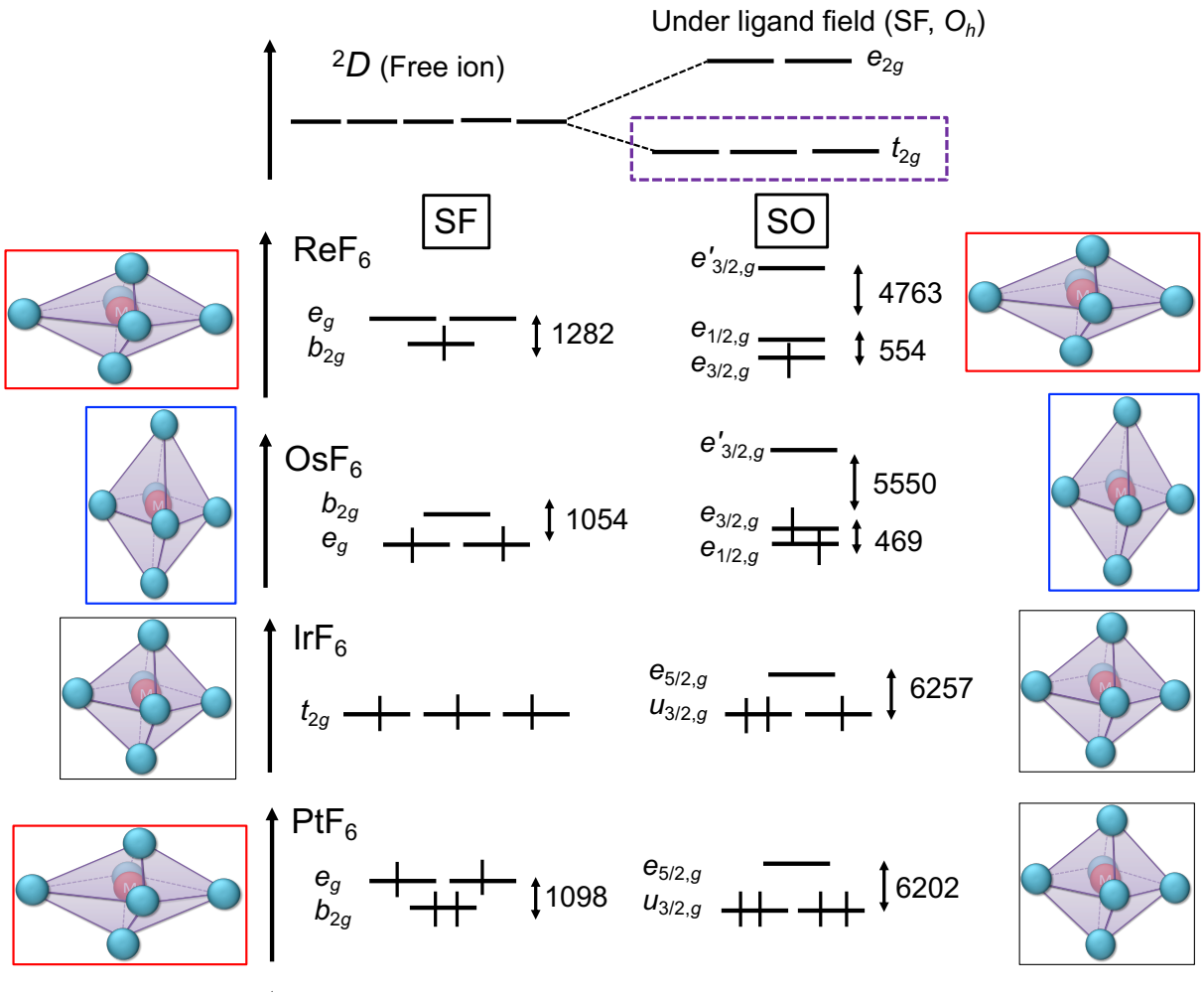

FIG. 1. Schematic orbital energy diagram and electronic configurations for t_{2g}-type orbitals at the SF and SO levels. In our notation, b_{2g} corresponds to d_{xy}-type orbital, where the z-axis is the axial axis of MF_6. Schematic molecular structures are also shown. The energy differences (cm^{-1}) and symmetry labels (Mulliken's symbol) are obtained at the X2C/AOC-HF/dyall.v3z level. Schematic electronic configurations are described based on the results at the X2C/MRCI/dyall.v3z level, employing the optimized geometries shown in Table V. The orbital energy differences are obtained with n ($1 \leq n \leq 4$) electrons in six t_{2g}-like orbitals and with 128 electrons in the closed orbitals. The option ".OPENFAC=1.0" is specified in the DIRAC calculations to satisfy Koopmans's theorem.

the spin-free (SF) and spin-orbit (SO) relativistic Hamiltonians. For the one-electron part of the Hamiltonian, the exact two-component Hamiltonian (X2C) [66] is employed for both SF and SO relativistic calculations. For the two-electron term, the non-relativistic Coulomb operator is employed for the SF calculation, and the Gaunt term is added in the atomic mean-field approximation (AMFI) [67] scheme for the SO calculation [68]. The nuclear potential is described by the Gauss-type finite-size nuclear model [69]. For all elements in this study, dyall.v3z basis sets [70–72] are employed in the uncontracted form.

The multi-reference configuration interaction (MRCI) theory was employed to compute the wavefunction for geometry optimization and vertical excitation energies. For the MRCI calculation, we employed the LUCITA module [73–75] for the SF Hamiltonian and the KRCI module [76–78] for the SO Hamiltonian. In these modules, one can flexibly specify the number of holes in the CI space, and this is called the general-active-space configuration-interaction (GASCI) method. The active space employed in this study is shown in Table I. Here, the complete-active-space CI (CASCI) calculation is employed in the space constructed by the t_{2g} orbitals in the SF or by the $u_{3/2,g}$ and $e_{5/2,g}$ orbitals in the SO levels (GAS2), and the two-electron excitation is allowed from the GAS2 space. One-electron excitations from GAS1 and GAS2 (a total of two electrons) are also allowed. The truncation of the virtual orbitals shown in Table II is determined so that the two orbitals are energetically well-separated. The same CI parameters are employed for both SO and SF calculations. The reference orbitals of the MRCI cal-

TABLE I. Generalized active space (GAS) models for CI wave functions of the MF_6 molecules. The parameters m and n that determine the occupation constraints of the subspaces are described in Table II

		accumulated # of electrons	
	# of orbitals	min	max
GAS3	m	$24+n$	$24+n$
GAS2	3	$22+n$	$24+n$
GAS1	12	23	24
frozen	(52)		

TABLE II. Parameter values for CI calculations of the MF_6 molecules. n refers to the number of correlated electrons of GAS2 space (t_{2g} orbitals in the SF and $u_{3/2,g}$ and $e_{5/2,g}$ orbitals in the SO). m refers to the number of virtual orbitals included in the GAS3 space. "small" is employed for the optimization, and "large" is employed for the excited state and JT distortion energy calculations

M	Re	Os	Ir	Pt	Au	Hg
n	1	2	3	4	5	6
m (small)	35	35	35	35	35	38
m (large)	62	62	65	69	-	-

culation are generated with the average-of-configuration Hartree-Fock (AOC-HF) method [79] or the HF method. The detailed parameters are listed in Table III.

We also employed the CCSD(T) method [80] for the optimization of HgF_6, assuming O_h symmetry. The 32 electrons from the highest occupied molecular orbital (HOMO) are correlated, and the virtual space is truncated at 5 Hartree.

Unless otherwise explicitly mentioned, we optimized the two axial and four equatorial M-F bonds of MF_6 molecules, assuming they belong to the O_h or D_{4h} symmetry group. The SURFIT program [81] was used to obtain the equilibrium structure in a two-dimensional potential energy surface for several molecules. Numerous one-point calculations were performed for the other molecules by changing the bond length by a step size of 0.001 Å. The details are explained in the Supporting Information. The O_h structure was obtained using the twofit program, which is a utility of the DIRAC code.

TABLE III. Parameter values to obtain the reference orbitals for the CI calculations of the MF_6 molecules provided in Table II at each relativistic Hamiltonian (REL). Only the central metal M is shown in the table. "closed" refers to the number of electrons occupied in the closed shell orbitals. m/n shown in "open" means that m electrons are distributed to n orbitals in the AOC-HF method. The HF method was employed when the open-shell electron was zero

REL	CI	shell	Re	Os	Ir	Pt	Au	Hg
SO	small	closed	128	128	128	132	132	134
		open	1/4	2/4	3/4	0	1/2	0
	large	closed	128	128	128	128	-	-
		open	1/6	2/6	3/6	4/6	-	-
SF	small	closed	128	128	128	128	132	134
		open	1/6	2/6	3/6	4/6	1/2	0
	large	closed	128	128	128	128	-	-
		open	1/6	2/6	3/6	4/6	-	-

TABLE IV. Optimized bond lengths of HgF_6 (r) in Å obtained using different methods. The dyall.v3z basis sets were employed.

method	CCSD(T)		MRCI		PBE0[36]	
X2C	SO	SF	SO	SF	SO[a]	SF
r	1.920	1.927	1.889	1.892	1.885	1.887

[a] The two-electron spin-orbit effect is simulated by a screened-nuclear-spin-orbit approach.

The projection analysis [82] using the intrinsic atomic orbital [83] was carried out for the PtF_6 molecule. At the SF level, two electrons are distributed in four orbitals, and 130 electrons occupy the closed shell in the AOC-HF calculation. In the projection analysis step, 0.01 and 1.99 electrons are distributed in the virtual e'_g and e_g orbitals and the occupied b_{2g} orbitals to obtain the gross population of the virtual e'_g orbitals. At the SO level, 132 electrons occupy the closed shell in the HF calculation. In the projection analysis step, 0.01 (3.99) electrons are distributed in the virtual $u'_{3/2,g}$ and $e_{5/2,g}$ orbitals (the occupied $u_{3/2,g}$ orbitals) (cf., Figure 2). In the atomic and molecular calculations, an option of the DIRAC code, .OPENFAC=1.0, was employed.

IV. RESULTS AND DISCUSSION

1. *Structures*

To estimate the dynamic correlation effect in the employed GAS scheme in the MRCI method, the bond lengths of HgF_6 obtained by the MRCI are compared with the CCSD(T) values (cf. Table IV). The symmetry of the HgF_6 molecule is fixed to O_h. From the comparison between the MRCI and CCSD(T) values, the MRCI method underestimates the dynamic correlation on the bond length by 0.031-0.035 Å. From the viewpoint of dynamic correlation, the MRCI provides similar accuracy to that of the PBE0 functional of DFT [36]. Although this deviation is similar in magnitude to the JT distortion (cf. Tables V and VII), it would not matter because the multi-reference effect would be more significant for determining the symmetry of the open-shell MF_6 systems. The MRCI and CCSD(T) methods provide the SO effects in a similar order of magnitude. This means that the coupling between the SO effect and the dynamic correlation would not affect the conclusion of our study.

The SO effect is not a correction of the SF calculation but can change the molecular point group symmetries at equilibrium geometry. Our results at the MRCI level are listed in Table V. The most sophisticated literature values at the SF-CCSD(T) and SO-BLYP levels are listed in Table VI. The geometries were obtained with several experimental methods [50, 51, 53, 54], but here we show

only one set of experimental values obtained by electron diffraction in the gas phase [52]. The space symmetry of IrF_6 is O_h at both the SF and SO levels, but the orbital is splitting at the SO level. The space symmetry of PtF_6 is changed at the SF (D_{4h}) and SO (O_h) levels, where the electronic structure becomes closed-shell. From the comparison between the SF-MRCI and SO-MRCI values, the SOC reduces the JT distortions of ReF_6 and OsF_6. This trend is not reported at the DFT level [33]. From the orbital energy levels shown in Figure 1, the SO splittings of ReF_6, OsF_6, and PtF_6 are larger than the splitting due to JT distortion at the SF level. Our bond lengths at the SF-MRCI level are smaller than those at the SF-CCSD(T) level shown in Table IV, while is consistent with the conclusion obtained from Table IV. The JT distortion reduced by the SO effect is also observed in the stabilization energy (cf. Table VII).

The electronic structure of AuF_6 may be different from the others. AuF_6 has ungerade-type orbitals with higher energies than t_{2g}-type orbitals, as shown in Figure S1 of the Supporting information. AuF_6 should not be explained like the other third-row transition metal fluorides. More careful investigation of the reference orbitals and active spaces is required, and thus, we do not study AuF_6 in the subsequent sections. The bond length of AuF_6 shown in Table V is different from the literature value, but we also found a local minimum of AuF_6 that is closer to the literature value (1.913 Å (×2) and 1.898 Å(×4) at the SF-X2C/MRCI/dyall.v3z level), which is 6354 cm^{-1} less stable than the one shown in Table V.

Similar schematic figures have been previously reported for group 10 hexafluorides [55, 56] and group 9 monoanionic hexafluorides [57] namely that d_4-type configurations predict octahedral symmetries, but they did not explicitly mention the triplet spin-state at the SF level. Furthermore, the influence of the SOC on the electron affinity (EA) discussed in ref 33 can also be rationalized with reference to Figure 1. By adding the SO correction, these authors demonstrated that the EA of OsF_6 becomes smaller than that of IrF_6. From Figure 1, the added electron predominantly occupies the $e_{5/2,g}$ spinor of IrF_6 in the SO level, which is energetically higher compared to the one at the SF level, where it occupies the triply degenerate t_{2g} orbitals.

A. Excitation spectra

Tables VIII and IX list the vertical excitation energy at the SF and SO levels. We could not simply correlate the states calculated at the SO level with the states without the SOC (SF calculations) except for the ReF_6 case, where ${}^2E_g \rightarrow E_{1/2,g}, E_{3/2,g}$ is observed. Even if the degeneracy of states is the same, the electronic structure can differ. This is exemplified by the ground state of IrF_6, which is the ${}^4A_{2g}$ and $U_{3/2,g}$ states at the SF and SO levels, respectively.

The molecular symmetry of the double group can be assigned as done in the point group at the NR level, using the direct product of the representation and Bethe's descending symmetry method [84, 85]. The total symmetry of ReF_6 with one valence electron corresponds to the occupied spinor. In the bosonic case (even number of electrons), whether D_{4h} (OsF_6) or O_h (PtF_6), the doubly degenerate states are E_g, and the closed-shell states are A_1. Regarding the non-degenerate states with an open-shell configuration for OsF_6, according to the direct product of the representation of orbitals in the double group (*e.g.*, refs 24, 86)

$$\begin{aligned} e_{1/2,g} \otimes e_{3/2,g} &= b_{1g} \oplus b_{2g} \oplus e_g \\ e_{3/2,g} \otimes e_{3/2,g} &= a_{1g} \oplus a_{2g} \oplus e_g \end{aligned} \tag{9}$$

b_{1g} and b_{2g} corresponds to $d_{x^2-y^2}$ and "d_{xy}" type basis sets, respectively. In addition, the Mulliken population analysis [87] at the one-component basis set level using the DIRAC code shows that "d_{xy}", d_{yz}, and d_{zx} orbitals contribute to $e_{1/2}$, $e_{3/2}$, and $e'_{3/2}$ spinors. a_{1g} does not contribute to an open-shell state. Based on these conditions, the states with $e_{1/2}(1)e_{3/2}(1)$ and $e_{3/2}(1)e_{3/2}(1)$ type configuration correspond to B_{1g} and A_{2g}, respectively. To distinguish the triply degenerate states of O_h, T_1, and T_2, we employed Bethe's method of descending symmetry [84, 85]. By going down to a lower symmetry, D_{4h}, the triple degeneracy splits as follows [86]:

$$\begin{aligned} T_{1g} &\rightarrow A_{2g} \oplus E_g \\ T_{2g} &\rightarrow B_{2g} \oplus E_g \end{aligned} \tag{10}$$

In other words, the A_{2g} (B_{2g}) states at the D_{4h} structure, which was calculated in slightly distorting the structure from O_h to D_{4h}, corresponds to the T_{1g} (T_{2g}) states. The A_{2g} and B_{2g} states in D_{4h} symmetry can be distinguished based on the occupation number of the spinor, as shown in eq 9. For IrF_6, a Fermionic system (odd number of electrons) in O_h symmetry, the quadruply degenerate states are always in $U_{3/2}$ symmetry. The doubly degenerate states ($E_{1/2}$ and $E_{5/2}$) can be distinguished from a doublet-like electronic configuration (one open-shell orbital, the others are closed-shell) in the CI wavefunction. The electronic configuration $[u_{3/2}(4),\ e_{1/2,6s}(1)]$ contributes to the $E_{1/2}$ state, where Ir's $6s$ orbital contributes to $e_{1/2,6s}$. In the $E_{5/2}$ state, a Kramers pair (two spinors) of four spinors in $u_{3/2}$ are occupied, and another electron occupies the $e_{5/2}$ spinor. The assignment at the SF level, which has been extensively investigated and thus will not be described here, was carried out based on the orbital occupation number under the C_{2v} symmetry using Bethe's method and the phase of the Slater determinants of the CI wavefunctions.

Although the experimental UV/vis spectra were reported [88, 89], vibrational calculations using more sophisticated electronic structure theory would be essential to compare with the experimental spectra. Further efforts are also needed to assign the experimental spectra. They are beyond the scope of the present study and will be pursued in future studies.

TABLE V. Bond lengths in Å, state and symmetry for metal hexafluorides at the most stable states calculated at X2C/MRCI/dyall.v3z level

	SO-MRCI	SF-MRCI
ReF_6	D_{4h} 1.785 (×2), 1.814 (×4)	$^2B_{2g}/D_{4h}$ 1.773 (×2), 1.820 (×4)
OsF_6	D_{4h} 1.819 (×2), 1.790 (×4)	$^3B_{2g}/D_{4h}$ 1.828 (×2), 1.785 (×4)
IrF_6	O_h 1.799	$^4A_{2g}/O_h$ 1.798
PtF_6	O_h 1.806	$^3B_{2g}/D_{4h}$ 1.774 (×2), 1.814 (×4)
AuF_6	O_h 1.839	$^2B_{2g}/D_{4h}$ 1.849 (×2), 1.796 (×4)

TABLE VI. Summary of the most sophisticated literature values for bond lengths (Å), state, and symmetry for metal hexafluorides and the experimental values in the gas phase

	SO-ZORA-BLYP [33]	SF-CCSD(T) [33]	exp. [52]
ReF_6	D_{4h} 1.899 (×2), 1.878 (×4)	$^2B_{2g}/D_{4h}$ 1.802 (×2), 1.844 (×4)	1.829(2)
OsF_6	D_{4h} 1.877 (×2), 1.892 (×4)	$^3A_{1g}/D_{4h}$ 1.856 (×2), 1.816 (×4)	1.828(2)
IrF_6	O_h 1.894	$^4A_{1g}/O_h$ 1.832	1.839(2)
PtF_6	D_{4h} 1.915 (×2), 1.909 (×4)[a]	$^3A_{1g}/D_{4h}$ 1.823 (×2), 1.856 (×4)	1.852(2)
AuF_6	O_h 1.936	$^2B_{2g}/D_{4h}$ 1.897 (×2), 1.878 (×4)	

[a] ref 56 reports O_h symmetry with 1.867 Å using the B3LYP functional based on the Dirac-Coulomb-Gaunt Hamiltonian.

TABLE VII. JT distortion energy (E_{JT} in cm^{-1}), which is the difference between the energy obtained at the optimized geometry shown in Table V and optimized bond length (r in Å) in O_h symmetry

	E_{JT}		r	
	SF	SO	SF	SO
ReF_6	415	123	1.804	1.804
OsF_6	364	71	1.799	1.800
PtF_6	369	-	1.801	-

B. Population analysis

Finally, the SO effect of the MF_6 is analyzed from the viewpoint of the atomic SO splitting. Figure 2 shows a schematic diagram of the ligand field splitting of the atomic d orbitals at the SF and SO levels as well as the gross population of the PtF_6. This figure is similar to Figures 19.4 and 19.5 of ref 58, but we added the gross population of PtF_6 obtained by the projection analysis at the X2C/HF/dyall.v3z level of theory in this study. The projection analysis is a method to obtain the contribution from the atomic orbital to the molecular orbital (MO) based on the two- or four-component Hamiltonian that can work with the one-component basis sets, as demonstrated in refs. [82, 90–93].

From the gross population, $5d_{5/2}$ ($5d_{3/2}$) contributes to the $u'_{3/2,g}$ ($u_{3/2,g}$) spinors more significantly. This means that the SO splitting at the atomic orbital level remains even under the ligand field, and the SO splitting changes the degeneracy behavior of the MOs. According to the Mulliken population analysis using the one-component basis sets, the d_{xy}, d_{yz}, and d_{xz} orbitals are distributed to the $e_{5/2,g}$ and $u_{3/2,g}$ orbitals, and d_{x^2}, d_{y^2}, and d_{z^2} contribute to $u'_{3/2,g}$ orbitals. Therefore, $u'_{3/2,g}$ orbitals would have similar properties to those of e'_g orbitals, although the assignments are different at the SF and SO levels. In fact, the total gross populations of d orbitals of $u'_{3/2,g}$ and e'_g have almost the same magnitude.

V. CONCLUSION

The geometry and excitation spectra of third-row transition metal hexafluorides are discussed based on the SF- and SO-X2C MRCI theory. The electronic states involved in the excitation spectra are assigned based on the double group. Including the SOC variationally in the X2C Hamiltonian allows for analysis of SO splitting at the MO level. Our schematic MO diagram can effectively demonstrate how the SOC influences the structures of the metal hexafluorides. From the comparison between the SF and SO results, the SOC dramatically changes a well-known picture of the ligand field without the SOC: triply degenerate t_{2g} orbitals are splitting to one $e_{5/2,g}$ and doubly degenerate $u_{3/2,g}$ orbitals. The SO effect should not be obtained as *a correction* using a single-reference method such as DFT in molecules with multi-reference characters. The SO splitting destroys the degeneracy of the MOs at the SF level and quenches the JT distortion. The excited states at the SO level cannot simply correlate to those at the SF level due to the strong SOC. A strong SO effect is also observed in the population analysis.

The observation in this study should be applicable to photochemistry [94] and spin chemistry [95] of heavy element systems. Further expansion of this study to the vibrational properties, including the dynamic JT effect, is also interesting. In the context of theoretical chemistry, these kinds of heavy metal complexes with high symmetry would be an attractive target for relativistic correlated theory aimed at strong correlation, such as density matrix renormalization group (DMRG) theory

TABLE VIII. Symmetry representations (sym), degeneracies (deg) for the energy levels, leading CI configurations, calculated vertical excitation energies in cm^{-1}, for ReF_6 and OsF_6 at the geometries shown in Table V. The orbital labels are shown in Figure 1. The integer in the parentheses is the occupation number. For example, *e.g.*, $e_{3/2,g}(2)$ refers to the $e_{3/2,g}$ orbitals occupied by two electrons

	SF				SO			
	sym	deg	configuration	energy	sym	deg	configuration	energy
ReF_6	$^2B_{2g}$	2	$b_{2g}(1)$	0	$E_{3/2,g}$	2	$e_{3/2,g}(1)$	0
	^2E_g	4	$e_g(1)$	1312	$E_{1/2,g}$	2	$e_{1/2,g}(1)$	566
					$E_{3/2,g}$	2	$e'_{3/2,g}(1)$	5304
OsF_6	$^3B_{2g}$	3	$e_g(2)$	0	A_{1g}	1	$e_{1/2,g}(2), e_{3/2,g}(2)$	0
	^3E_g	6	$e_g(1)b_{2g}(1)$	1100	E_g	2	$e_{1/2,g}(1)e_{3/2,g}(1)$	241
	$^1B_{2g}$	1	$e_g(2)$	8490	B_{2g}	1	$e_{1/2,g}(1)e_{3/2,g}(1)$	444
	$^1A_{1g}$	1	$e_g(2)$	8677	B_{2g}	1	$e_{1/2,g}(1)e_{3/2,g}(1)$	587
	^1E_g	2	$e_g(1)b_{2g}(1)$	9643	E_g	2	$e_{1/2,g}(1)e'_{3/2,g}(1)$	4944
	$^1A_{1g}$	1	$e_g(2), b_{2g}(2)$	9946	A_{2g}	1	$e_{3/2,g}(1)e'_{3/2,g}(1)$	5290
	$^1A_{1g}$	1	$e_g(2), b_{2g}(2)$	20873	A_{1g}	1	$e_{1/2,g}(2), e_{3/2,g}(2)$ $e'_{3/2,g}(2)$	5666
					B_{2g}	1	$e_{1/2,g}(1)e'_{3/2,g}(1)$	11548
					B_{2g}	1	$e_{1/2,g}(1)e'_{3/2,g}(1)$	11860
					E_g	2	$e_{3/2,g}(1)e'_{3/2,g}(1)$	12278
					A_{2g}	1	$e_{3/2,g}(1)e'_{3/2,g}(1)$	12676
					A_{1g}	1	$e'_{3/2,g}(2)$	24299

TABLE IX. Symmetry representations (sym), degeneracies (deg) for the energy levels, leading CI configurations, calculated vertical excitation energies in cm^{-1}, for ReF_6 and OsF_6 at the geometries shown in Table V. The orbital labels are shown in Figure 1. The integer in the parentheses is the occupation number. For example, *e.g.*, $u_{3/2,g}(3)$ refers to the $u_{3/2,g}$ orbitals occupied by three electrons

	SF				SO			
	sym	deg	configuration	energy	sym	deg	configuration	energy
IrF_6	$^4A_{2g}$	4	$t_{2g}(3)$	0	$U_{3/2,g}$	4	$u_{3/2,g}(3)$	0
	^2E_g	4	$t_{2g}(3)$	11945	$U_{3/2,g}$	4	$u_{3/2,g}(3)$, $u_{3/2,g}(2)e_{5/2,g}(1)$	11054
	$^2T_{1g}$	6	$t_{2g}(3)$	12685	$U_{3/2,g}$	4	$u_{3/2,g}(2)e_{5/2,g}(1)$	12911
	$^2T_{2g}$	6	$t_{2g}(3)$	19701	$E_{1/2,g}$	2	$u_{3/2,g}(2)e_{5/2,g}(1)$	13529
					$E_{5/2,g}$	2	$u_{3/2,g}(2)e_{5/2,g}(1)$	20816
					$U_{3/2,g}$	4	$u_{3/2,g}(1)e_{5/2,g}(2)$	23184
PtF_6	$^3B_{2g}$	3	$b_{2g}(2)e_g(2)$	0	A_{1g}	1	$u_{3/2,g}(4)$	0
	^3E_g	6	$b_{2g}(1)e_g(3)$	943	T_{2g}	3	$u_{3/2,g}(3)e_{5/2,g}(1)$	4039
	$^1B_{2g}$	1	$b_{2g}(2)e_g(2)$	7203	T_{1g}	3	$u_{3/2,g}(3)e_{5/2,g}(1)$	6945
	^1E_g	2	$b_{2g}(1)e_g(3)$	8092	E_g	2	$u_{3/2,g}(3)e_{5/2,g}(1)$, $u_{3/2,g}(2)e_{5/2,g}(2)$	7283
	$^1A_{1g}$	1	$b_{2g}(2)e_g(2)$	9030	T_{1g}	3	$u_{3/2,g}(2)e_{5/2,g}(2)$ [a]	14872
	$^1A_{1g}$	1	$b_{2g}(2)e_g(2), e_g(4)$	10743	E_g	2	$u_{3/2,g}(2)e_{5/2,g}(2)$	16797
	$^1A_{1g}$	1	$b_{2g}(2)e_g(2), e_g(4)$	19793	A_{1g}	1	$u_{3/2,g}(2)e_{5/2,g}(2)$ [b]	26698

[a] The excitation from the GAS1 to GAS2 spaces also contributes.
[b] The excitation from the GAS2 to GAS3 spaces also contributes.

[96, 97], driven similarity renormalization group (DSRG) theory [98], and DMRG-tailored coupled cluster theory [99]. Feature calculations using these theories may provide results closer to the experimental ones. This study also provides fundamental knowledge about the chemistry of heavy metal complexes. The results would serve as useful examples for a lecture on inorganic chemistry.

ACKNOWLEDGMENTS

The author thanks financial support from the JSPS KAKENHI (grant no 21K14643) and JST Moonshot R&D (Grant No. JPMJMS2269). The author used the computer resource offered under the category of General Projects by the Research Institute for Information Technology, Kyushu University, and the FUJITSU Supercomputer PRIMEHPC FX1000 and FUJITSU Server PRIMERGY GX2570 (Wisteria/BDEC-01) at the Information Technology Center, The University of Tokyo.

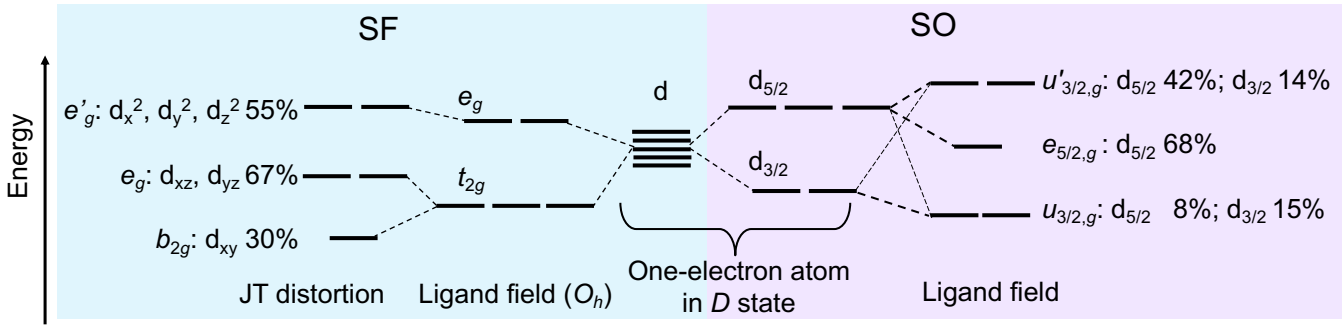

FIG. 2. Schematic diagram of the ligand field splitting of the atomic d orbital at the SF and SO levels. The gross population of the Pt 5d orbitals in PtF_6 obtained by the projection analysis are also shown.

The author thanks Kirk Peterson (Washington State) for allowing us to use the SURFIT program. The author thanks Editage (`www.editage.com`) for English language editing.

VI. SUPPLEMENTAL MATERIALS

The following Supporting Information is available free of charge.

- MF6_suppl.pdf: Details of the optimization and the schematic orbital energy diagrams, including the AuF_6 molecule

[1] G. L. Miessler, P. J. Fischer, and D. A. Tarr, *Inorganic chemistry fifth edition* (New York: Pearson Education, Inc, 2014).
[2] F. Albert Cotton, G. Wilkinson, C. A. Murillo, and M. Bochmann, *Advanced Inorganic Chemistry* (John Wiley & Sons, 1999).
[3] C. E. Housecroft and A. G. Sharpe, *Inorganic Chemistry* (Pearson Education, 2005).
[4] H. A. Jahn, E. Teller, and F. G. Donnan, Stability of polyatomic molecules in degenerate electronic states - I—Orbital degeneracy, Proceedings of the Royal Society of London. Series A - Mathematical and Physical Sciences **161**, 220 (1937).
[5] T. Kambara, Theory of high-spin $\rightleftharpoons$ low-spin transitions in transition metal compounds induced by the Jahn–Teller effect, J. Chem. Phys. **70**, 4199 (1979).
[6] M. Maiss and C. A. M. Brenninkmeijer, Atmospheric SF6: Trends, sources, and prospects, Environ. Sci. Technol. **32**, 3077 (1998).
[7] Z. Cui, Y. Li, S. Xiao, S. Tian, J. Tang, Y. Hao, and X. Zhang, Recent progresses, challenges and proposals on SF_6 emission reduction approaches, Sci. Total Environ. **906**, 167347 (2024).
[8] N. Bartlett, The oxidizing properties of the third transition series hexafluorides and related compounds, Angew. Chem. Int. Ed Engl. **7**, 433 (1968).
[9] R. C. Burns and T. A. O'Donnell, Reactivity of transition metal fluorides—x. oxidation-reduction reactions of rhenium, osmium and iridium hexafluorides, J. Inorg. Nucl. Chem. **42**, 1285 (1980).
[10] K. O. Christe, W. W. Wilson, and R. D. Wilson, Coordinatively saturated fluoro cations. oxidative fluorination reactions with fluorokrypton(1+) salts and platinum hexafluoride (PtF6), Inorg. Chem. **23**, 2058 (1984).
[11] A. A. Orlov, A. F. Tsimbalyuk, and R. V. Malyugin, Desublimation for purification and transporting UF_6: Process description and modeling, Sep. Purif. Rev. **46**, 81 (2017).
[12] J. K. Gibson and W. A. d. Jong, *Experimental and Theoretical Approaches to Actinide Chemistry*, edited by J. K. Gibson and W. A. de Jong (John Wiley & Sons, Ltd, Chichester, UK, 2018).
[13] K. Seppelt, Molecular hexafluorides, Chem. Rev. **115**, 1296 (2015).
[14] P. Pyykko, Relativistic effects in structural chemistry, Chemical Reviews **88**, 563 (1988).
[15] P. Schwerdtfeger, ed., *Relativistic Electronic Structure Theory, Part 1. Fundamentals* (Elsevier, 2002).
[16] K. G. Dyall and K. Fægri Jr, *Introduction to relativistic quantum chemistry* (Oxford University Press, 2007).
[17] M. Barysz and Y. Ishikawa, *Relativistic Methods for Chemists* (Springer Netherlands, 2010).
[18] T. Saue, Relativistic Hamiltonians for chemistry: A primer, ChemPhysChem **12**, 3077 (2011).
[19] M. Reiher and A. Wolf, *Relativistic quantum chemistry: the fundamental theory of molecular science* (John Wiley & Sons, 2014).
[20] J. C. Phillips and L. Kleinman, New method for calculating wave functions in crystals and molecules, Phys. Rev. **116**, 287 (1959).
[21] P. Schwerdtfeger, J. R. Brown, J. K. Laerdahl, and H. Stoll, The accuracy of the pseudopotential approxi-

mation. III. a comparison between pseudopotential and all-electron methods for au and AuH, J. Chem. Phys. **113**, 7110 (2000).
[22] P. Schwerdtfeger, The pseudopotential approximation in electronic structure theory, Chemphyschem **12**, 3143 (2011).
[23] M. Dolg and X. Cao, Relativistic pseudopotentials: Their development and scope of applications, Chem. Rev. **112**, 403 (2012).
[24] R. Boca, *A handbook of magnetochemical formulae* (Elsevier Science Publishing, Philadelphia, PA, 2012).
[25] E. Miyoshi and Y. Sakai, Theoretical study on electronic structures of AuF6 and its anions, J. Chem. Phys. **89**, 7363 (1988).
[26] S. A. Macgregor and K. H. Moock, Stabilization of high oxidation states in transition metals. 2.1 WCl_6 oxidizes $[WF_6]^-$, but would $PtCl_6$ oxidize $[PtF_6]^-$? an electrochemical and computational study of 5d transition metal halides: $[MF_6]$z versus $[MCl_6]^z$ (m = ta to pt; z = 0, 1-, 2-), Inorg. Chem. **37**, 3284 (1998).
[27] K. G. Dyall, Bond dissociation energies of the tungsten fluorides and their singly charged ions: A density functional survey, J. Phys. Chem. A **104**, 4077 (2000).
[28] R. Wesendrup and P. Schwerdtfeger, Structure and electron affinity of platinum fluorides, Inorg. Chem. **40**, 3351 (2001).
[29] S. Riedel and M. Kaupp, Where is the limit of highly fluorinated high-oxidation-state osmium species?, Inorg. Chem. **45**, 10497 (2006).
[30] S. Riedel, Platinum fluorides beyond PtF6?, J. Fluor. Chem. **128**, 938 (2007).
[31] M. Straka, P. Hrobarik, and M. Kaupp, Understanding structure and bonding in early actinide $6d^05f^0$ MX (m) Th-Np; X) h, f) complexes in comparison with their transition metal 5d analogues (2008).
[32] R. Craciun, R. T. Long, D. A. Dixon, and K. O. Christe, Electron affinities, fluoride affinities, and heats of formation of the second row transition metal hexafluorides: MF6 (m = mo, tc, ru, rh, pd, ag), J. Phys. Chem. A **114**, 7571 (2010).
[33] R. Craciun, D. Picone, R. T. Long, S. Li, D. A. Dixon, K. A. Peterson, and K. O. Christe, Third row transition metal hexafluorides, extraordinary oxidizers, and lewis acids: electron affinities, fluoride affinities, and heats of formation of WF_6, ReF_6, OsF_6, IrF_6, PtF_6, and AuF_6, Inorg. Chem. **49**, 1056 (2010).
[34] A. K. Srivastava and N. Misra, Theoretical investigation on the structure, stability and superhalogen properties of OsF_n (n=1–7) species, J. Fluor. Chem. **158**, 65 (2014).
[35] A. K. Srivastava, S. K. Pandey, and N. Misra, Superhalogen properties of ReF_n ($n \geq 6$) species, Chem. Phys. Lett. **624**, 15 (2015).
[36] C. Gao, S.-X. Hu, H. Han, G. Guo, B. Suo, and W. Zou, Exploring the electronic structure and stability of HgF_6: Exact 2-component (X2C) relativistic DFT and NEVPT2 studies, Computational and Theoretical Chemistry **1160**, 14 (2019).
[37] T. Graubner, A. J. Karttunen, and F. Kraus, A computational study on Closed-Shell molecular hexafluorides MF_6 (M=S, se, te, po, xe, rn, cr, mo, w, u) - molecular structure, anharmonic frequency calculations, and prediction of the NdF6 molecule, Chemphyschem **24**, e202200903 (2023).
[38] S. Hu and W. Zou, Stable copernicium hexafluoride (CnF_6) with an oxidation state of +VI, Phys. Chem. Chem. Phys. **19**, 10.1039/d1cp04360a (2021).
[39] D. Dai, S. Roszak, and K. Balasubramanian, Electronic states of the hafnium trimer (hf_3), Chem. Phys. Lett. **308**, 495 (1999).
[40] K. Balasubramanian and D. Majumdar, Spectroscopic properties of lead trimer (pb3 and pb3+): Potential energy surfaces, spin-orbit and Jahn-Teller effects, J. Chem. Phys. **115**, 8795 (2001).
[41] C. Zhao and K. Balasubramanian, Spectroscopic properties of lead hexamer and its ions (pb_6, pb_6^+, pb_6^-), J. Chem. Phys. **116**, 10287 (2002).
[42] R. Guo, K. Balasubramanian, X. Wang, and L. Andrews, Infrared vibronic absorption spectrum and spin–orbit calculations of the upper spin–orbit component of the au3 ground state, J. Chem. Phys. **117**, 1614 (2002).
[43] P. Mondal, D. Opalka, L. V. Poluyanov, and W. Domcke, Jahn-Teller and spin-orbit coupling effects in transition-metal trifluorides, Chem. Phys. **387**, 56 (2011).
[44] P. Mondal, D. Opalka, L. V. Poluyanov, and W. Domcke, Ab initio study of dynamical E × e Jahn-Teller and spin-orbit coupling effects in the transition-metal trifluorides TiF_3, CrF_3, and NiF_3, J. Chem. Phys. **136**, 084308 (2012).
[45] S. Koseki, T. A. Hisashima, T. Asada, A. Toyota, and N. Matsunaga, Tetrahydrides of third-row transition elements: Spin-orbit coupling effects on the stability of rhenium tetrahydride, J. Chem. Phys. **133**, 10.1063/1.3495680 (2010).
[46] T. A. Hisashima, T. Matsushita, T. Asada, S. Koseki, and A. Toyota, Tetra-hydrides of the third-row transition elements: Spin-orbit coupling effects on geometrical deformation in WH_4 and OsH_4, Theor. Chem. Acc. **120**, 85 (2008).
[47] J. Gaunt, The vibrational spectrum and molecular structure of rhenium hexafluoride, Trans. Faraday Soc. **50**, 209 (1954).
[48] B. Weinstock, H. H. Claassen, and J. G. Malm, Vibrational spectra of OsF_6 and PtF_6, J. Chem. Phys. **32**, 181 (1960).
[49] M. J. Molski and K. Seppelt, The transition metal hexafluorides, Dalton Trans. , 3379 (2009).
[50] E. J. Jacob and L. S. Bartell, Electron diffraction study of rhenium fluorides. i. heavy-atom corrections and structure of ReF_6, J. Chem. Phys. **53**, 2231 (1970).
[51] M. Kimura, V. Schomaker, D. W. Smith, and B. Weinstock, Electron-diffraction investigation of the hexafluorides of tungsten, osmium, iridium, uranium, neptunium, and plutonium, J. Chem. Phys. **48**, 4001 (1968).
[52] A. D. Richardson, K. Hedberg, and G. M. Lucier, Gas-phase molecular structures of third row transition-metal hexafluorides WF_6, ReF_6, OsF_6, IrF_6, and PtF_6. an electron-diffraction and ab initio study, Inorg. Chem. **39**, 2787 (2000).
[53] T. Drews, J. Supeł, A. Hagenbach, and K. Seppelt, Solid state molecular structures of transition metal hexafluorides, Inorg. Chem. **45**, 3782 (2006).
[54] S. A. Brewer, A. K. Brisdon, J. H. Holloway, and E. G. Hope, EXAFS STUDIES ON SOLUTIONS OF METAL HEXAFLUORIDES IN AN-HYDROUS HF, Plan. Perspect. **749**, 152 (1994).
[55] J. David, P. Fuentealba, and A. Restrepo, Relativistic

effects on the hexafluorides of group 10 metals, Chem. Phys. Lett. **457**, 42 (2008).
[56] L. Alvarez-Thon, J. David, R. Arratia-Pérez, and K. Seppelt, Ground state of octahedral platinum hexafluoride, Phys. Rev. A **77**, 034502 (2008).
[57] J. David, D. Guerra, and A. Restrepo, The Jahn-Teller effect: A case of incomplete theory for d 4 complexes?, Inorg. Chem. **50**, 1480 (2011).
[58] M. S. Dresselhaus, G. Dresselhaus, and A. Jorio, *Applications of group theory to the physics of solids* (Springer New York, 2008).
[59] D. Majumdar, S. Roszak, and J. Leszczynski, Relativistic symmetries in the electronic structure and properties of molecules, in *Relativistic Methods for Chemists*, edited by M. Barysz and Y. Ishikawa (Springer Netherlands, Dordrecht, 2010) pp. 373–405.
[60] E. Pavarini, crystal-field theory , tight-binding method and jahn-teller effect, Correlated electrons: from models to materials **2**, 6 (2012).
[61] J. J. Sakurai and J. Napolitano, *Modern quantum mechanics* (Cambridge University Press, 2020).
[62] R. Shankar, *Principles of Quantum Mechanics* (Springer US, 2012).
[63] DIRAC, a relativistic ab initio electronic structure program, Release DIRAC22 (2022), written by H. J. Aa. Jensen, R. Bast, A. S. P. Gomes, T. Saue and L. Visscher et al. (available at `http://dx.doi.org/10.5281/zenodo.6010450`, see also `http://www.diracprogram.org`), accessed May 05, 2024.
[64] T. Saue, R. Bast, A. S. P. Gomes, H. J. A. Jensen, L. Visscher, I. A. Aucar, R. Di Remigio, K. G. Dyall, E. Eliav, E. Fasshauer, *et al.*, The DIRAC code for relativistic molecular calculations, J. Chem. Phys. **152**, 204104 (2020).
[65] A. Sunaga, Structure and Excitation Spectra of Third-Row Transition Metal Hexafluorides Based on Multi-Reference Exact Two-Component Theory, Zenodo `https://doi.org/10.5281/zenodo.11531162` (2024), the dataset for the ab inito calculation associated with this manuscript is available at the zenodo repository.
[66] M. Iliaš and T. Saue, An infinite-order two-component relativistic hamiltonian by a simple one-step transformation, J. Chem. Phys. **126**, 64102 (2007).
[67] (), aMFI, an atomic mean-field spin-orbit integral program, 1996, Bernd Schimmelpfennig, University of Stockholm.
[68] (), after we started this study, a more elaborated picture-change scheme for the two-electron terms in the two-component Hamiltonians was reported [100], but the traditional AMFI scheme works well for valence orbitals [18].
[69] L. Visscher and K. G. Dyall, Dirac–Fock atomic electronic structure calculations using different nuclear charge distributions, At. Data Nucl. Data Tables **67**, 207 (1997).
[70] K. G. Dyall, Relativistic double-zeta, triple-zeta, and quadruple-zeta basis sets for the 5d elements Hf-Hg, Theoretical Chemistry Accounts **112**, 403–409 (2004).
[71] K. G. Dyall and A. S. Gomes, Revised relativistic basis sets for the 5d elements Hf-Hg, Theoretical Chemistry Accounts **125**, 97–100 (2010).
[72] K. G. Dyall, Relativistic double-zeta, triple-zeta, and quadruple-zeta basis sets for the light elements H–Ar, Theor. Chem. Acc. **135**, 128 (2016).
[73] J. Olsen, P. Jørgensen, and J. Simons, Passing the one-billion limit in full configuration-interaction (FCI) calculations, Chem. Phys. Lett. **169**, 463 (1990).
[74] T. Fleig and L. Visscher, Large-scale electron correlation calculations in the framework of the spin-free dirac formalism: The au2molecule revisited, Chem. Phys. **311**, 113 (2005).
[75] S. Knecht, H. J. A. Jensen, and T. Fleig, Large-scale parallel configuration interaction. i. nonrelativistic and scalar-relativistic general active space implementation with application to (Rb-Ba)+, J. Chem. Phys. **128**, 014108 (2008).
[76] T. Fleig, J. Olsen, and L. Visscher, The generalized active space concept for the relativistic treatment of electron correlation. II. Large-scale configuration interaction implementation based on relativistic 2- and 4-spinors and its application, J. Chem. Phys. **119**, 2963 (2003).
[77] S. Knecht, H. J. A. Jensen, and T. Fleig, Large-scale parallel configuration interaction. II. Two- and four-component double-group general active space implementation with application to BiH, J. Chem. Phys. **132**, 014108 (2010).
[78] Stefan R. Knecht. Parallel Relativistic Multiconfiguration Methods: New Powerful Tools for Heavy-Element Electronic-Structure Studies. PhD thesis, Mathematisch-Naturwissenschaftliche Fakultät, Heinrich-Heine-Universität Düsseldorf, 2009. URL: http://docserv.uni-duesseldorf.de/servlets/DocumentServlet?id=13226.
[79] Jørn Thyssen. Development and Applications of Methods for Correlated Relativistic Calculations of Molecular Properties. PhD thesis, University of Southern Denmark, 2001. URL: http://dirac.chem.sdu.dk/thesis/thesis-jth2001.pdf.
[80] L. Visscher, T. J. Lee, and K. G. Dyall, Formulation and implementation of a relativistic unrestricted coupled-cluster method including noniterative connected triples, J. Chem. Phys. **105**, 8769–8776 (1996).
[81] J. Senekowitsch, Ph.D. dissertation, Universität Frankfurt, Frankfurt, Germany, 1988.
[82] S. Dubillard, J.-B. Rota, T. Saue, and K. Faegri, Bonding analysis using localized relativistic orbitals: Water, the ultrarelativistic case and the heavy homologues H_2X (X=Te, Po, eka-Po), J. Chem. Phys. **124**, 154307 (2006).
[83] G. Knizia, Intrinsic Atomic Orbitals: An Unbiased Bridge between Quantum Theory and Chemical Concepts, J. Chem. Theory Comput. **9**, 4834 (2013).
[84] H. Bethe, Termaufspaltung in kristallen, Ann. Phys. **395**, 133 (1929).
[85] C. J. Ballhausen, *Introduction to ligand field theory* (1962).
[86] S. L. Altmann and P. Herzig, *Point-group theory tables* (1994).
[87] R. S. Mulliken, Electronic population analysis on LCAO–MO molecular wave functions. I, J. Chem. Phys. **23**, 1833 (1955).
[88] W. Moffitt, G. L. Goodman, M. Fred, and B. Weinstock, The colours of transition metal hexafluorides, Mol. Phys. **2**, 109 (1959).
[89] T. Chemnitz, B. N. Koch, M. R. Buchner, W. Petry, and F. Kraus, Plasmachemical syntheses of RuF6, RhF6,

and PtF6, Inorg. Chem. **62**, 16263 (2023).
[90] S. Knecht, S. Fux, R. van Meer, L. Visscher, M. Reiher, and T. Saue, Mössbauer spectroscopy for heavy elements: a relativistic benchmark study of mercury, Theor. Chem. Acc. **129**, 631 (2011).
[91] A. Oleynichenko, A. Zaitsevskii, S. Romanov, L. V. Skripnikov, and A. V. Titov, Global and local approaches to population analysis: Bonding patterns in superheavy element compounds, Chem. Phys. Lett. **695**, 63 (2018).
[92] M. Iliaš and V. Pershina, Carbonyl compounds of rh, ir, and mt: electronic structure, bonding and volatility, Phys. Chem. Chem. Phys. **22**, 18681 (2020).
[93] A. Sunaga, C. Tabata, and T. Yamamura, Linearity and chemical bond of UO22+ revisited: A comparison study with UN_2 and UE_2^{2+} (e = s, se, and te) based on relativistic calculations, J. Phys. Chem. A **126**, 8606 (2022).
[94] W. R. Kitzmann, J. Moll, and K. Heinze, Spin-flip luminescence, Photochem. Photobiol. Sci. **21**, 1309 (2022).
[95] P. J. Hore, K. L. Ivanov, and M. R. Wasielewski, Spin chemistry, J. Chem. Phys. **152**, 120401 (2020).
[96] C. E. Hoyer, H. Hu, L. Lu, S. Knecht, and X. Li, Relativistic Kramers-Unrestricted Exact-Two-Component density matrix renormalization group, J. Phys. Chem. A **126**, 5011 (2022).
[97] H. Zhai, H. R. Larsson, S. Lee, Z.-H. Cui, T. Zhu, C. Sun, L. Peng, R. Peng, K. Liao, J. Tölle, J. Yang, S. Li, and G. K.-L. Chan, Block2: A comprehensive open source framework to develop and apply state-of-the-art DMRG algorithms in electronic structure and beyond, J. Chem. Phys. **159**, 10.1063/5.0180424 (2023).
[98] Z. Zhao and F. A. Evangelista, Towards accurate spin-orbit splittings from relativistic multireference electronic structure theory, arXiv:2405.0607 (2024), arXiv:2405.06077 [cond-mat.str-el].
[99] J. Brandejs, J. Višňák, L. Veis, M. Maté, Ö. Legeza, and J. Pittner, Toward DMRG-tailored coupled cluster method in the 4c-relativistic domain, J. Chem. Phys. **152**, 174107 (2020).
[100] S. Knecht, M. Repisky, H. J. A. Jensen, and T. Saue, Exact two-component hamiltonians for relativistic quantum chemistry: Two-electron picture-change corrections made simple, J. Chem. Phys. **157**, 114106 (2022).